

Angular distribution of γ -rays from a neutron-induced p -wave resonance of ^{132}Xe

T. Okudaira,¹ Y. Tani,² S. Endo,^{1,3} J. Doskow,⁴ H. Fujioka,² K. Hirota,^{1,*} K. Kameda,²
A. Kimura,³ M. Kitaguchi,¹ M. Luxnat,⁴ K. Sakai,³ D. Schaper,⁵ T. Shima,⁶ H. M. Shimizu,¹
W. M. Snow,⁴ S. Takada,^{7,†} T. Yamamoto,¹ H. Yoshikawa,⁶ and T. Yoshioka⁷

¹Nagoya University, Furocho, Chikusa, Nagoya 464-8602, Japan

²Tokyo Institute of Technology, Meguro, Tokyo 152-8551, Japan

³Japan Atomic Energy Agency, 2-1 Shirane, Tokai 319-1195, Japan

⁴Indiana University, Bloomington, IN 47401, USA

⁵Los Alamos National Laboratory, Los Alamos, NM 87545, USA

⁶Osaka University, Ibaraki, Osaka 567-0047, Japan

⁷Kyushu University, 744 Motoooka, Nishi, Fukuoka 819-0395, Japan

(Dated: December 22, 2022)

A neutron-energy dependent angular distribution was measured for individual γ -rays from the 3.2 eV p -wave resonance of $^{131}\text{Xe}+n$, that shows enhanced parity violation owing to a mixing between s - and p -wave amplitudes. The γ -ray transitions from the p -wave resonance were identified, and the angular distribution with respect to the neutron momentum was evaluated as a function of the neutron energy for 7132 keV γ -rays, which correspond to a transition to the 1807 keV excited state of ^{132}Xe . The angular distribution is considered to originate from the interference between s - and p -wave amplitudes, and will provide a basis for a quantitative understanding of the enhancement mechanism of the fundamental parity violation in compound nuclei.

PACS numbers: 13.75.Cs, 21.10.Hw, 21.10.Jx, 21.10.Re, 23.20.En, 24.30.Gd, 24.80.+y, 25.40.Fq, 25.70.Gh, 27.60.+j, 29.30.Kv

Keywords: compound nuclei, partial wave interference, neutron radiative capture reaction

I. INTRODUCTION

Parity odd asymmetries on the order of 10^{-6} have been observed in the helicity dependence of the scattering cross section in nucleon-nucleon scattering experiments [1–3]. This tiny parity violation is understood to come from the weak amplitude in the hadronic interaction, which is on the order of $10^{-6} - 10^{-7}$ times the strong amplitude. In the neutron absorption reaction of nuclei with a mass number of around 100, large parity violations with sizes of up to 10% have been observed on p -wave resonances located on the tail of s -wave resonances. The fundamental parity violation in the nucleon-nucleon interaction is enhanced by the mixing between s - and p -wave amplitudes of compound nuclei, referred to as the s - p mixing model [4, 5].

The interference terms between s - and p -wave amplitudes introduced by the s - p mixing model implies several correlations between neutron momentum, neutron polarization, γ -ray momentum, and γ -ray polarization at the p -wave resonance [6]. These correlations provide important information needed to understand the enhancement mechanism of the parity violation in compound nuclei (e.g. partial neutron width and weak matrix element). They are measured as a neutron-energy dependent angular distributions of emitted γ -rays

from p -wave resonances. Non-uniform angular distributions were observed in reactions of $^{139}\text{La}(n,\gamma)^{140}\text{La}^*$ [7], $^{139}\text{La}(n,\gamma)^{140}\text{La}_{g.s.}$ [8], $^{139}\text{La}(\vec{n},\gamma)^{140}\text{La}_{g.s.}$ [9] and $^{117}\text{Sn}(n,\gamma)^{118}\text{Sn}_{g.s.}$ [10], $^{117}\text{Sn}(\vec{n},\gamma)^{118}\text{Sn}_{g.s.}$ [11]. Fundamental time reversal violation can be enhanced by the same mechanism, and these nuclei can be utilized to search for T-violation in the nucleon-nucleon interaction by measuring a forward scattering amplitude with polarized neutrons and a polarized or aligned nuclear target [12].

The 3.2 eV p -wave resonance of $^{131}\text{Xe}+n$ is an important compound state in the study of the s - p mixing model and the search for new physics. A very large parity-odd longitudinal asymmetry with a size of $(4.3 \pm 0.2)\%$ was observed in the 3.2 eV p -wave resonance of $^{131}\text{Xe}+n$ with a neutron transmission measurement [13]. This parity violation is the second largest for p -wave resonances in the eV region, where high neutron intensity can be obtained at spallation sources, after $(9.56 \pm 0.35)\%$ for ^{139}La [14]. A ^{131}Xe nuclear polarization of $7.6 \pm 1.5\%$ using spin exchange optical method (SEOP) was also recently achieved [15].

The (n, γ) measurement in Ref. [16] suggested that the 3.2 eV p -wave resonance originates from $^{131}\text{Xe}+n$, but no detailed study of the p -wave resonance with γ -ray measurements has been performed since then. The 3.2 eV p -wave resonance has a very small cross section, which requires a large neutron beam intensity and large solid angle of γ -ray detectors. Also, there is a very large 14.4 eV s -wave resonance in $^{131}\text{Xe}+n$ (2.0×10^4 barn) near the p -wave resonance. γ -rays from a very large 14.4 eV s -wave resonance saturate γ -ray detectors, and thus it is

* Present Address: High Energy Accelerator Research Organization, 1-1 Oho, Tsukuba, Ibaraki 305-0801, Japan

† Present Address: Tohoku University, 41 Kawauchi, Aoba-ku, Sendai, 980-8576 Japan

difficult to increase the neutron beam intensity. In this paper, we report the angular distribution of the γ -rays from the 3.2 eV p -wave resonance with a high statistics by employing an enriched ^{131}Xe filter upstream of the detector array, that selectively absorbs incident neutrons around 14.4 eV to avoid the detector saturation around the p -wave resonance.

II. EXPERIMENT

A. Experimental Setup

The $^{131}\text{Xe}(n, \gamma)^{132}\text{Xe}$ reaction was measured with a pulsed epithermal neutron beam at Accurate Neutron-Nucleus Reaction Measurement Instrument (ANNRI) beamline of the Material and Life Science Experimental Facility (MLF) of the Japan Proton Accelerator Research Complex (J-PARC). The neutron induced prompt γ -rays were measured with 22 germanium detectors. The germanium detectors are oriented at angles from 36° to 144° with respect to the incident neutron beam direction [17]. The neutron beam was collimated to 22 mm using epithermal neutron collimators installed upstream of the germanium detectors. The detailed description of the beamline is given in Ref. [8].

The experimental setup is shown in Fig. 1. The nuclear target was 84.4% enriched ^{131}Xe gas. The Xe gas was encapsulated into a cylindrical cell with a pressure of 0.43 MPa, a diameter of 49 mm and a thickness of 76 mm. The target was placed at the detector center, and the distance from the moderator surface to the Xe target was 21.5 m. The ^{131}Xe filter was an 84.4% enriched ^{131}Xe gas encapsulated with a pressure of 0.79 MPa at room temperature in a cylindrical aluminum cell with an inner diameter of 23 mm and a thickness of 500 mm. It was installed inside the collimator, and the distance from the moderator surface to the center of the ^{131}Xe filter was 20.0 m. Most of incident neutrons around the s -wave resonance were absorbed by the ^{131}Xe filter, whereas the neutrons around 3.2 eV passed through it because of the small cross section of the p -wave resonance. A cadmium filter with 1 mm thickness was installed to absorb thermal neutrons. As we shall see later, γ -rays of $^{56}\text{Fe}(n, \gamma)^{57}\text{Fe}$ reactions from the upstream of the beamline was the main background in this experiment. A lead filter was used to suppress γ -ray background, moderately sacrificing the neutron beam intensity. Measurements were performed under two different γ -ray backgrounds and neutron beam intensities with 37.5 mm-thick and 50 mm-thick lead filters. The proton beam power was 600 kW and the total measurement time was 227 hours.

B. Measurement

We measured the energy deposition and the arrival time of the capture γ -rays event-by-event in a list mode.

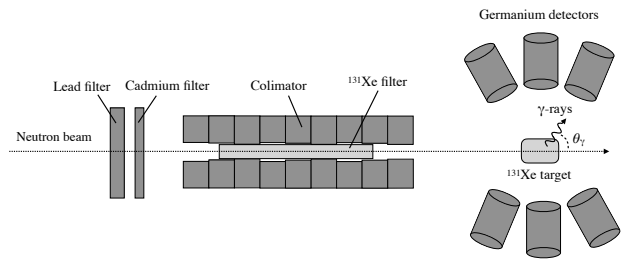


FIG. 1. Experimental setup.

The energy deposition of γ -rays in the germanium detector E_γ^m is determined from the pulse height.

The time-of-flight of the incident neutrons was obtained using the arrival time of the γ -rays t^m from intense γ -flash emitted during the proton spallation reactions in the target. The corresponding neutron energy E_n^m is calculated using t^m and the known beamline geometry. The neutron energy in the center-of-mass system E_n is defined as well. The total number of γ -ray events detected in the experiment are denoted as I_γ . A 2-dimensional histogram corresponding to $\partial^2 I_\gamma / \partial t^m \partial E_\gamma^m$ was obtained for each germanium crystal. The detailed definitions of variables are described in Ref. [8].

An incident beam spectrum for t^m , obtained from a measurement of the 477.6 keV γ -rays in the neutron absorption reaction of ^{10}B with an enriched ^{10}B target, is shown in Fig. 2. Figure 2 shows that the incident neutrons were selectively suppressed around the s -wave resonances of $\text{Xe}+n$ due to neutron absorption reactions in the ^{131}Xe filter.

The histogram of $\partial I_\gamma / \partial t^m$ measured with the ^{131}Xe target is shown in Fig. 3. The small peak at $t^m \sim 880 \mu\text{s}$ is the 3.2 eV p -wave resonance of $^{131}\text{Xe}+n$, and the peak at $t^m \sim 410 \mu\text{s}$ corresponds to the 14.4 eV s -wave resonance of $^{131}\text{Xe}+n$, which is strongly suppressed by the ^{131}Xe filter. We corrected for 10% and 5% of the total γ -ray signals overlapped in time in the measurements with a 37.5 mm and 50 mm lead filter, respectively [8].

Figure 4 shows a γ -ray spectrum defined as $\partial I_\gamma / \partial E_\gamma^m$, which is integrated for $t^m < 0 \mu\text{s}$. The γ -ray spectrum gated with $2.98 \text{ eV} < E_n^m < 3.42 \text{ eV}$, which corresponds to the energy range of the p -wave resonance, is also shown in Fig. 5. Note that the γ -rays from the s -wave component and other backgrounds were subtracted in Fig. 5 by estimating the s -wave and backgrounds components with a third polynomial fit in the histogram of $\partial I_\gamma / \partial t^m$. The transitions from the p -wave resonance were identified from Fig. 5 for the first time and the decay scheme for the 3.2 eV p -wave resonance was obtained as shown in Fig. 6. The energy levels of ^{132}Xe were taken from Ref. [19]. The 7132 keV γ -ray, which corresponds to the transition to 1804 keV excited state of ^{132}Xe , was observed as a direct transition from the 3.2 eV p -wave resonance. The 7132 keV γ -ray had not been found in previous studies,

r	published values					this work		
	E_r [eV]	J_r	l_r	Γ_r^γ [meV]	$2g_r\Gamma_r^n$ [meV]	$2g_r\Gamma_r^{n/l_r}$ [meV]	E_r [eV]	Γ_r^γ [meV]
1	-5.41	(1)		123.7		2.93		
2	3.2 ± 0.3		1		$(3.2 \pm 0.3) \times 10^{-5}$		3.20 ± 0.01	174 ± 7
3	14.41 ± 0.014	(2)	0	93.5 ± 6.2	268 ± 7			

TABLE I. The resonance parameters of $^{131}\text{Xe}+n$ for low energy neutrons. The resonance parameters E_r , J_r , l_r , Γ_r^γ , g_r , and Γ_r^n are resonance energy, total angular momentum, orbital angular momentum, γ width, g -factor and neutron width, respectively. Parameter r denotes the resonance number. The spin and parity of ^{131}Xe are $3/2^+$, and therefore the p -wave resonance has negative parity. Published values are taken from Ref. [18].

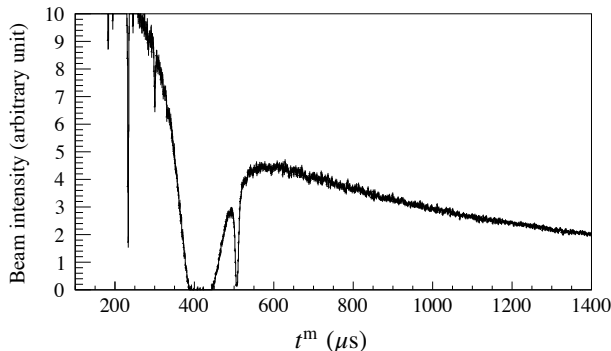


FIG. 2. Relative incident neutron spectrum as a function of t^m measured with the boron target. The neutron intensity around $410 \mu\text{s}$ and $500 \mu\text{s}$, which correspond to the peak energies of the 14.4 eV s -wave resonance of $^{131}\text{Xe}+n$ and 9.66 eV s -wave resonance of $^{129}\text{Xe}+n$, respectively, was reduced owing to the neutron absorber.

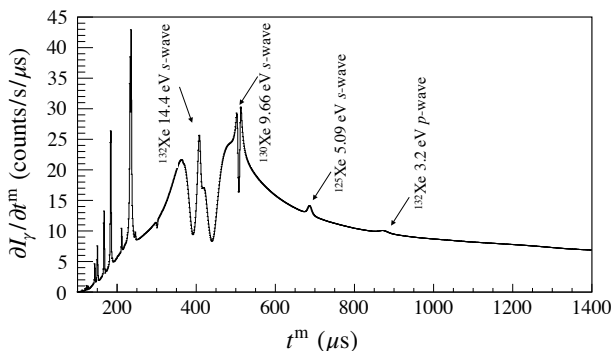


FIG. 3. γ -ray counts as a function of t^m with the ^{131}Xe target. The peak at $410 \mu\text{s}$ is considered to originate from neutrons passing through the gap between the collimator and the ^{131}Xe filter.

which focused on the s -wave component and the thermal region.[20–22].

The full absorption peak and the single escape peak of the 7132 keV γ -rays were used in the study of the angular distribution of γ -rays. The expanded γ -ray spectra integrated for $t^m > 0 \mu\text{s}$ and gated with the p -wave resonance are shown in Fig. 7. The main background for this study comes from the single and the double escape peaks of 7631 keV and 7646 keV γ -rays of the $^{56}\text{Fe}(n,\gamma)^{57}\text{Fe}$ reac-

tion, which arises from iron material used in the beamline instrument. These γ -ray peaks from $^{56}\text{Fe}+n$ cannot be isolated in the γ -ray spectrum because the peaks completely overlap with the full absorption and single escape peaks of 7132 keV γ -rays as shown in Fig. 7. The background subtraction was performed in the histogram of $\partial I_\gamma/\partial t^m$ for the evaluation of the angular distribution, which is described in subsection C.

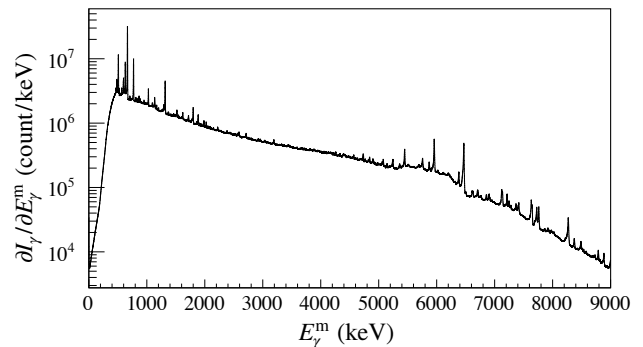


FIG. 4. γ -ray spectrum defined as $\partial I_\gamma/\partial E_\gamma^m$.

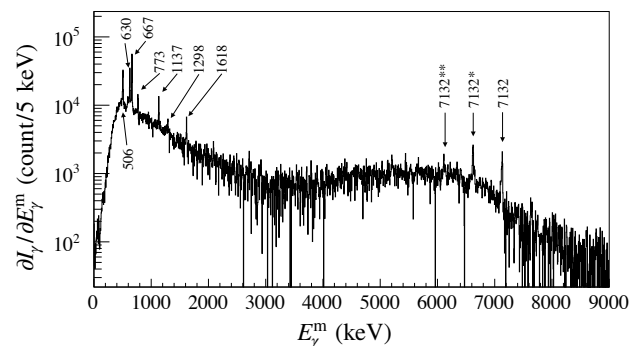


FIG. 5. γ -ray spectrum gated with the 3.2 eV p -wave component. The γ -ray energies of each peak are also shown. Single and double asterisks indicate single- and double-escape peaks, respectively. The origin of the γ -ray peak at 1618 keV was not identified in this study. The detection threshold was around 500 keV

The resonance parameters of the p -wave resonance

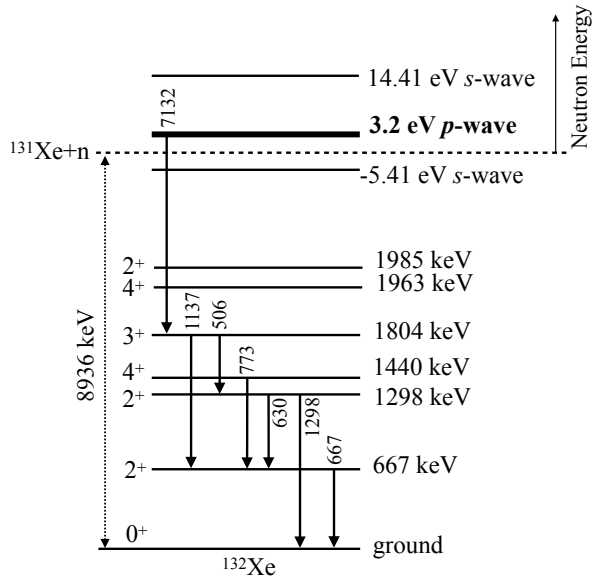


FIG. 6. Decay scheme from the 3.2 eV p -wave resonance of $^{131}\text{Xe}+n$ to ^{132}Xe . The dashed line shows separation energy of $^{131}\text{Xe}+n$. The excited states less than 2000 keV are depicted.

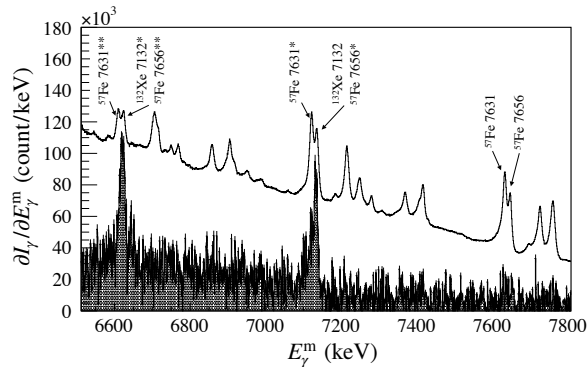


FIG. 7. Expanded γ -ray spectra around the 7132 keV γ -ray peak. The black line and shaded area denote the histograms integrated for $t^m > 0 \mu\text{s}$ and gated with the p -wave resonance, respectively. Single and double asterisks indicate single- and double- escape peaks, respectively. The single and double escape peaks from $^{56}\text{Fe}(n,\gamma)^{57}\text{Fe}$ overlap with the full absorption and single escape peaks of the 7132 keV γ -rays from $^{131}\text{Xe}(n,\gamma)^{132}\text{Xe}$. The histogram gated with the p -wave resonance is scaled by a factor of 200.

were determined with the histogram of $\partial I_\gamma/\partial t^m$ gated with the full absorption and single escape peaks of 7132 keV γ -rays. The p -wave resonance was fitted including the background and s -wave component with the Breit-Wigner function and $1/v$ components after the normalization by the incident neutron-beam spectrum. The fitting result and obtained fitting parameters are shown in Fig. 8 and Table I, respectively. The broadening of the resonance shape derived from the thermal motion of gas atoms and the pulse shape of the

neutron beam was taken into account in the fit. For the detailed formula of the fitting function, see APPENDIX (C),(D),and (E) in Ref. [8]. Because the neutron width of the p -wave resonance is negligibly smaller than the γ width of the p -wave resonance, the total width of the p -wave resonance was used as the γ -ray width of the p -wave resonance.

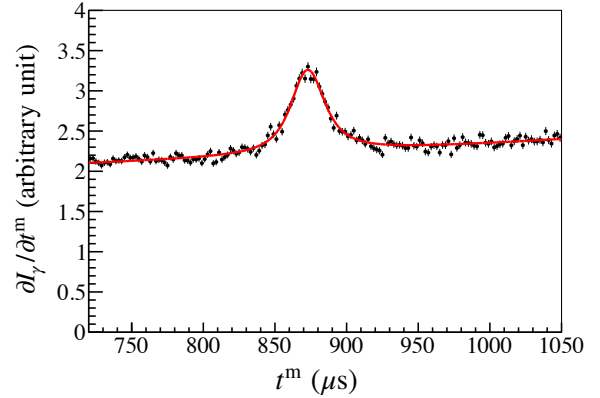


FIG. 8. Histogram of $\partial I_\gamma/\partial t^m$ gated with the full absorption and single escape peaks of 7132 keV γ -rays. The best fit is shown in the solid line.

C. Angular Distribution

The interference of the s -wave and p -wave amplitudes results in an asymmetric shape of the p -wave resonance, which is dependent on the angle, as has been observed in case of ^{140}La . [8]. The background component needs to be subtracted before the evaluation of the shape of the p -wave resonance. Since the neutron absorption reaction of ^{56}Fe does not have neutron resonances for $E_n < 1\text{keV}$, the 3.2 eV p -wave resonance of $^{131}\text{Xe}+n$ was isolated from the s -wave component of $^{131}\text{Xe}+n$ and a smooth background with a fit using $f(t^m) = at^m + b$ with free parameters a and b . For example, a histogram of $\partial I_\gamma/\partial t^m$ gated with the full absorption peak of 7132 keV after normalization of the incident neutron beam and fitting result are shown in Fig. 9. The region of the p -wave resonance was excluded in the fitting. The p -wave resonance after the subtraction of the s -wave and background components for each detector angle is shown in Fig. 10.

The angular distribution of the p -wave resonance shape is measured by a "low-high asymmetry" defined as

$$A_{\text{LH}}^p(\theta_d) = \frac{N_{\text{L}}^p(\theta_d) - N_{\text{H}}^p(\theta_d)}{N_{\text{L}}^p(\theta_d) + N_{\text{H}}^p(\theta_d)}, \quad (1)$$

where θ_d is the emission angle with respect to the incident neutron momentum, and N_{L}^p and N_{H}^p are integrals in the region of $E_2 - 1.5\Gamma_2 \leq E_n \leq E_2$ and

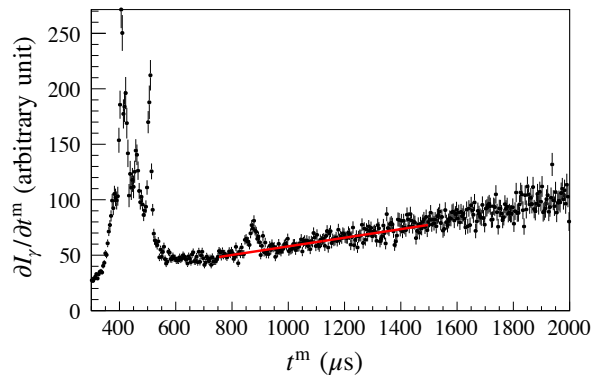


FIG. 9. Histogram of $\partial I_\gamma/\partial t^m$ gated with the full absorption peak of 7132 keV γ -rays for the single germanium crystal. The solid line shows the fit result of the s -wave and background components.

$E_2 \leq E_n \leq E_2 + 1.5\Gamma_2$, respectively. Variables E_2 and Γ_2 denote the resonance energy and total width of the p -wave resonance, which is defined by the γ width and neutron width shown in Table I as $\Gamma_2 = \Gamma_2^\gamma + \Gamma_2^n$. The detailed definitions of N_L^p and N_H^p are shown in Eq. (8) in Ref. [8] and Fig. 14 in Ref. [8]. Note that $A_{LH}^p(\theta_d)$, N_L^p and N_H^p are calculated only for the p -wave resonance.

The low-high asymmetry is plotted against the effective detector angle θ_d , which is obtained with a simulation of the germanium detector assembly [23], and fitted using a function of $A_{LH}^p(\theta_d) = A^p \cos \theta_d + B^p$ with free parameters A^p and B^p . The angular distributions of A_{LH}^p are obtained under the following four conditions: (1) the full absorption peak with the 37.5 mm thick lead filter, (2) the single escape peak with the 37.5 mm thick lead filter, (3) the full absorption peak with the 50.0 mm thick lead filter, (4) the single escape peak with the 50.0 mm thick lead filter, as shown in Fig. 11. The slope parameters A^p , which corresponds to the angular dependence of p -wave resonance shape, are plotted for the four conditions in Fig. 12. These results are consistent with each other,

and their average value was $A^p = 0.148 \pm 0.043$. The present result of the angular distribution is considered as an evidence of the interference between s - and p -wave amplitudes as already found in ^{140}La and ^{118}Sn [7–10].

III. CONCLUSION

The γ -rays from the $^{131}\text{Xe}(n, \gamma)^{132}\text{Xe}$ reaction, especially for the 3.2 eV p -wave resonance, was studied with high statistics by using the enriched ^{131}Xe target and filter. The γ -transition from the p -wave resonance state to the 3^+ state at 1804 keV was clearly observed as well as already known γ -transitions in ^{132}Xe . The neutron-energy dependent angular distribution was evaluated with the low-high asymmetry using the direct transition, and slope parameter A^p was determined to be 0.148 ± 0.043 . This result will be interpreted by combining with the results of ^{140}La and ^{118}Sn in terms of the s - p mixing model for a more detailed understanding of the enhancement mechanism of the symmetry violation. The combined analysis will be reported in a separate paper.

ACKNOWLEDGMENTS

The authors would like to thank the staff of beamline04 for the maintenance of the germanium detectors, and MLF and J-PARC for operating the accelerators and the neutron production target. The neutron scattering experiment was approved by the Neutron Scattering Program Advisory Committee of IMSS and KEK (Proposals Nos. 2014S03, 2015S12, 2018S12). The neutron experiment at the Materials and Life Science Experimental Facility of the J-PARC was performed under a user program (Proposal Nos. 2019A0113, 2020B0356, 2020B0451). This work was supported by JSPS KAKENHI Grant Nos. 17H02889, and the US National Science Foundation PHY-1913789. W. M. Snow acknowledges support from the Indiana University Center for Spacetime Symmetries.

-
- [1] J. M. Potter, J. D. Bowman, C. F. Hwang, J. L. McKibben, R. E. Mischke, D. E. Nagle, P. G. Debrunner, H. Frauenfelder, and L. B. Sorensen, Phys. Rev. Lett. **33**, 1307 (1974).
 - [2] V. Yuan, H. Frauenfelder, R. W. Harper, J. D. Bowman, R. Carlini, D. W. MacArthur, R. E. Mischke, D. E. Nagle, R. L. Talaga, and A. B. McDonald, Phys. Rev. Lett. **57**, 1680 (1986).
 - [3] E. G. Adelberger and W. C. Haxton, Ann. Rev. Nucl. Part. Sci. **35**, 501 (1985).
 - [4] O. P. Sushkov and V. V. Flambaum, Usp. Fiz. Nauk **136**, 3 (1982).
 - [5] O. P. Sushkov and V. V. Flambaum, Sov. Phys. Uspekhi **25**, 1 (1982).
 - [6] V. V. Flambaum and O. P. Sushkov, Nucl. Phys. A **435**, 352 (1985).
 - [7] T. Okudaira, S. Endo, H. Fujioka, K. Hirota, K. Ishizaki, A. Kimura, M. Kitaguchi, J. Koga, Y. Niinomi, K. Sakai, T. Shima, H. M. Shimizu, S. Takada, Y. Tani, T. Yamamoto, H. Yoshikawa, and T. Yoshioka, Phys. Rev. C **104**, 014601 (2021).
 - [8] T. Okudaira, S. Takada, K. Hirota, A. Kimura, M. Kitaguchi, J. Koga, K. Nagamoto, T. Nakao, A. Okada, K. Sakai, H. M. Shimizu, T. Yamamoto, and T. Yoshioka, Phys. Rev. C **97**, 034622 (2018).
 - [9] T. Yamamoto, T. Okudaira, S. Endo, H. Fujioka, K. Hirota, T. Ino, K. Ishizaki, A. Kimura, M. Kitaguchi, J. Koga, S. Makise, Y. Niinomi,

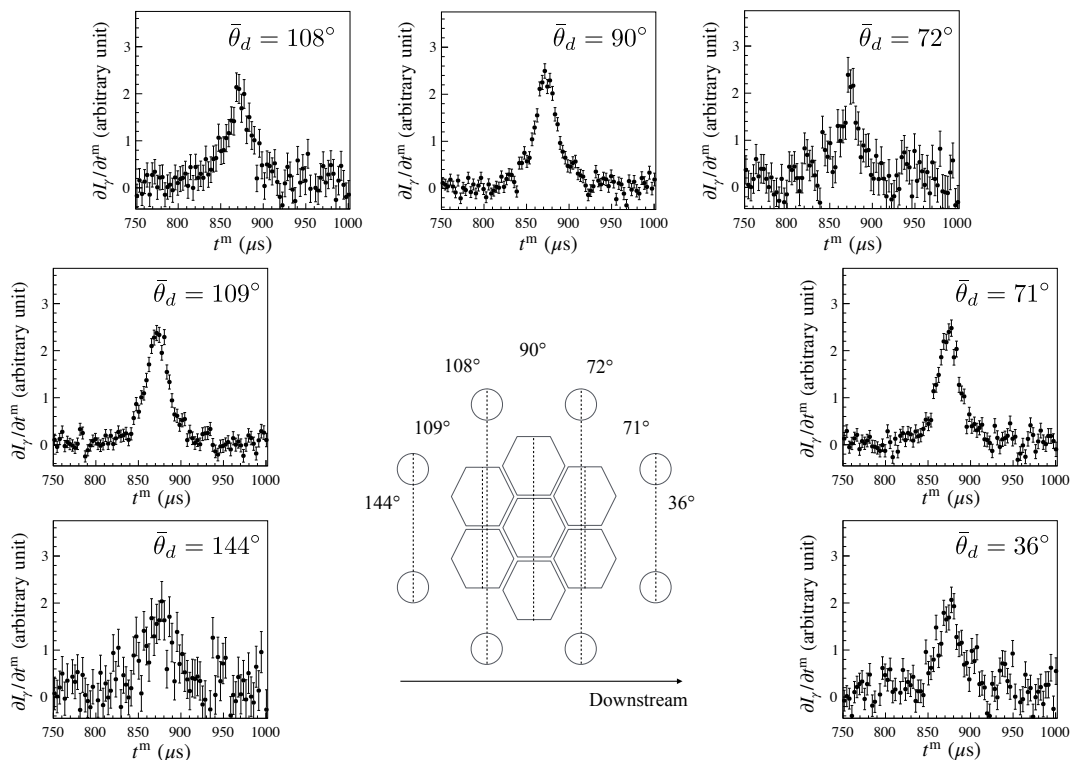


FIG. 10. Histograms of $\partial I_\gamma/\partial t^m$ gated with the single escape peak of 7132 keV γ -rays. The angles of the detector are denoted on the right top in each histograms.

- T. Oku, K. Sakai, T. Shima, H. M. Shimizu, S. Takada, Y. Tani, H. Yoshikawa, and T. Yoshioka, *Phys. Rev. C* **101**, 064624 (2020).
- [10] J. Koga, S. Takada, S. Endo, H. Fujioka, K. Hirota, K. Ishizaki, A. Kimura, M. Kitaguchi, Y. Niinomi, T. Okudaira, K. Sakai, T. Shima, H. M. Shimizu, Y. Tani, T. Yamamoto, H. Yoshikawa, and T. Yoshioka, *Phys. Rev. C* **105**, 054615 (2022).
- [11] S. Endo, T. Okudaira, R. Abe, H. Fujioka, K. Hirota, A. Kimura, M. Kitaguchi, T. Oku, K. Sakai, T. Shima, H. M. Shimizu, S. Takada, S. Takahashi, T. Yamamoto, H. Yoshikawa, and T. Yoshioka, *Phys. Rev. C* **106**, 064601 (2022).
- [12] V. P. Gudkov, *Phys. Rep.* **212**, 77 (1992).
- [13] J. J. Szymanski, W. M. Snow, J. D. Bowman, B. Cain, B. E. Crawford, P. P. J. Delheij, R. D. Hartman, T. Haseyama, C. D. Keith, J. N. Knudson, A. Komives, M. Leuschner, L. Y. Lowie, A. Masaike, Y. Matsuda, G. E. Mitchell, S. I. Penttilä, H. Postma, D. Rich, N. R. Roberson, S. J. Seestrom, E. I. Sharapov, S. L. Stephenson, Y. F. Yen, and V. W. Yuan, *Phys. Rev. C* **53**, R2576 (1996).
- [14] V. W. Yuan, C. D. Bowman, J. D. Bowman, J. E. Bush, P. P. J. Delheij, C. M. Frankle, C. R. Gould, D. G. Haase, J. N. Knudson, G. E. Mitchell, S. Penttilä, H. Postma, N. R. Roberson, S. J. Seestrom, J. J. Szymanski, and X. Zhu, *Phys. Rev. C* **44**, 2187 (1991).
- [15] M. J. Molway, L. Bales-Shaffer, K. Ranta, D. Basler, M. Murphy, B. E. Kidd, A. T. Gafar, J. Porter, K. Albin, B. M. Goodson, E. Y. Chekmenev, M. S. Rosen, W. M. Snow, J. Ball, E. Sparling, M. Prince, D. Cocking, and M. J. Barlow, (2021), 10.48550/ARXIV.2105.03076.
- [16] V. Skoy, E. Sharapov, N. Gundorin, Y. P. Popov, Y. V. Prokofichev, N. Roberson, and G. Mitchell, *Phys. Rev. C* **53**, R2573 (1996).
- [17] A. Kimura, T. Fujii, S. Fukutani, K. Furutaka, S. Goko, K. Y. Hara, H. Harada, K. Hirose, J. Hori, M. Igashira, T. Kamiyama, T. Katabuchi, T. Kin, K. Kino, F. Kitatani, Y. Kiyonagi, M. Koizumi, M. Mizumoto, S. Nakamura, M. Ohta, M. Oshima, K. Takamiya, and Y. Toh, *J. Nucl. Sci. Tech.* **49**, 708 (2012).
- [18] S. F. Mughabghab, *Atlas of Neutron Resonances 5th ed.* (Elsevier, Amsterdam, 2006).
- [19] N. Nica, *Nuclear Data Sheets* **108**, 1287 (2007).
- [20] W. Gelletly, W. R. Kane, and D. R. MacKenzie, *Phys. Rev. C* **3**, 1678 (1971).
- [21] L. V. Groshev, L. I. Govor, A. M. Demidov, and A. S. Rakhimov, *Yad.Fiz.* **13**, 1129 (1971).
- [22] S. A. Hamada, W. D. Hamilton, and B. More, *Journal of Physics G: Nuclear Physics* **14**, 1237 (1988).
- [23] S. Takada, T. Okudaira, F. Goto, K. Hirota, A. Kimura, M. Kitaguchi, J. Koga, T. Nakao, K. Sakai, H. M. Shimizu, T. Yamamoto, and T. Yoshioka, *Journal of Instrumentation* **13**, P02018 (2018).

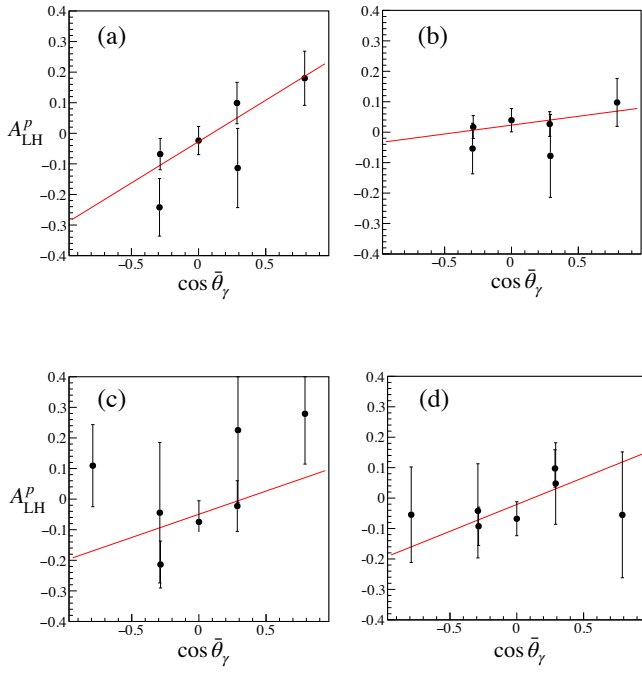


FIG. 11. Angular distributions of A_{LH}^P measured with the full absorption peak and single escape peak using the 37.5 mm and 50.0 mm thick lead filters. (a), (b), (c), and (d) indicate the full absorption peak with the 37.5 mm thick lead filter, the single escape peak with the 37.5 mm thick lead filter, the full absorption peak with the 50.0 mm thick lead filter, and the single escape peak with the 50.0 mm thick lead filter, respectively. In the graphs of (a) and (b), the detectors at 144° were not used in the fit because of the large dead time.

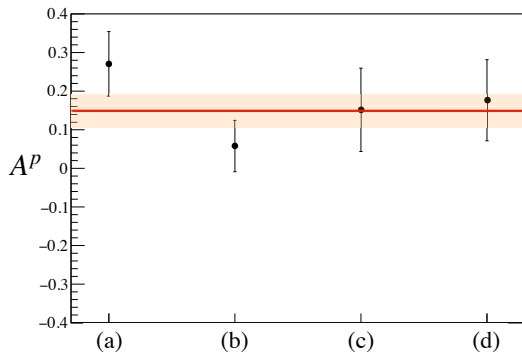


FIG. 12. The values of the angular dependence A^P for each condition. The solid line and colored region show the average value and 1σ region, respectively.